The Royal Society

The geometry of unfolding tree leaves

H. Kobayashi†, B. Kresling‡ and J. F. V. Vincent*

Centre for Biomimetics, The University of Reading, Reading RG6 6AT, UK

Leaves of hornbeam (*Carpinus betulus*) and beech (*Fagus sylvaticus*) were modelled to a first approximation as plane surfaces, with straight parallel folds, using numerical methods. In both species the lateral veins, when the leaves are outstretched, are angled at 30–50° from the centre vein. A higher angle allows the leaf to be folded more compactly within the bud, but it takes longer to expand. This may allow the plant to optimize the timing of leaf deployment with ecological and physiological conditions.

Keywords: Miura-Ori, unfolding, leaf opening, deployable structure, solar panel

1. INTRODUCTION

The leaves of most plants are folded or rolled while still inside the bud. Leaves of hornbeam and beech have relatively simple and regular corrugated folding patterns and mechanisms, which can suggest ideas for the design of deployable structures such as solar panels and lightweight antennae of satellites, or for the folding of deployable membranes such as tents, clothes or other coverings. Deployable structures have been studied for use in aerospace (Unda *et al*. 1994). A two-dimensional expandable array was proposed by Miura (1980) for a solar panel whose folding pattern has been called 'Miura-Ori' (Miura & Natori 1985). A thin membrane wrapped around a central hub was examined by Guest & Pellegrino (1992) as a design for a solar sail. Several concepts of deployable aerospace structure have been described (Miura 1993).

A number of biological folding patterns have been investigated, concentrating on mechanisms for stiffening and deployment. A series of studies using a cylindrical shell model based on a biological structure (Calladine 1978) was carried out by Guest & Pellegrino (1994*a*,*b*, 1996). The force required to fold the cylinder was examined theoretically and experimentally using a model consisting of identical triangular panels along a helical strip. Wing folding of insects has also been investigated (Wootton 1981; Kesel 1994; Brackenbury 1994). The geometry and mechanics of wing folding of Coleoptera have been studied using vector analysis (Haas 1994). Although many folding patterns can be found in plant structures (Delarue 1991; Kresling 1991, 1995), there have been few studies from a mechanical point of view.

We describe the unfolding of a leaf with a straight central (primary, main) vein and symmetrically arranged parallel lateral (secondary) veins that generate a corrugated surface. This morphology is relatively simple, so the description seems to be suited to the first step in the study of leaf folding. Numerical models with different angles between main and secondary veins were made to simulate the unfolding of such a corrugated leaf. Using vector analysis, angles of laminar element planes divided by creases and locations of creases, which correspond to veins, and the development of leaf area during unfolding, were calculated.

*Author for correspondence (szsvinct@reading.ac.uk).
†Present address: Mechanical Systems Engineering, Muroran Institute of Technology, Mizumoto, Muroran, 050, Japan.
‡Present address: Bionics and Experimental Design, 170 Rue St Charles, 75015 Paris, France.

2. OBSERVATION OF UNFOLDING LEAVES

Unfolding leaves are shown in figure 1 (common beech, *Fagus sylvaticus*) and figure 2 (hornbeam, *Carpinus betulus*). The leaves develop within a bud where they are protected by several layers of bud scales. In spring, the folded leaves emerge, revealing their regular folding pattern. Because the creases or folds in these leaves are along the veins the vein angle, α (defined as the angle between the midrib and the vein) and the location of the veins, X (measured from the boundary between the petiole and the leaf lamella), were measured for two specimens of both leaves (figure 3). We used a non-dimensional parameter, X^*, ($X^* = X/L_0$ where L_0 is the length of the lamina) to characterize the position of the veins. The vein angles in beech and hornbeam are not constant, but decrease gradually from about 50–30° towards the tip of the leaf. The average vein angle is about 40° in leaves of both species. The veins transport water and assimilation products within the leaf and provide mechanical support (Herbig & Kull 1991), so their geometry may be related to either of these functions.

3. NUMERICAL SIMULATION OF LEAF UNFOLDING

(a) *The model leaf and coordinate system*

To simulate the unfolding of a regularly corrugated simple leaf, we consider a paper model with crest and valley creases (figure 4). This pattern is a simple form of a developable double corrugation surface called 'Miura-Ori'. One of the most interesting properties of this pattern is that it allows simultaneous extension in two directions perpendicular to each other.

We made a number of assumptions and limitations in the simulation: (1) folding and unfolding are symmetrical about the midrib; (2) corrugated folding is regular (the distance between creases, and the inclined angle of the creases, corresponding to the vein angles, α, are constant along the length of the leaf); (3) the folds cannot store

© 1998 The Royal Society
Received 18 September 1997 *Accepted* 22 September 1997

Figure 1. Unfolding manner of common beech leaves: (*a*) a bud, (*b*) buds just after opening, (*c*) an early stage of unfolding, and (*d*) corrugated leaves.

Figure 2. Unfolding manner of leaves of hornbeam: (*a*) a bud, (*b*) buds just after opening, (*c*) an early stage of unfolding, and (*d*) corrugated leaves.

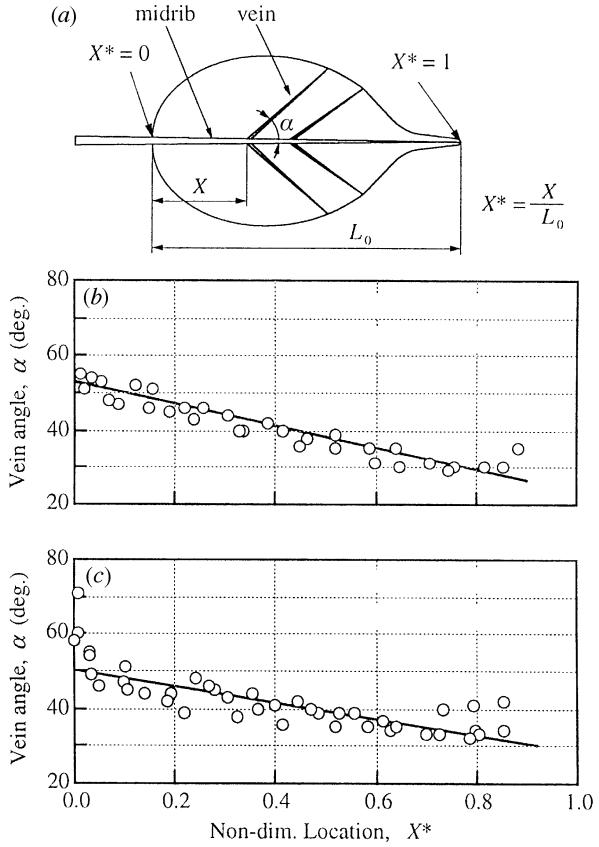

Figure 3. Vein angles measured in two leaves, each of common beech and hornbeam. (*a*) Schematic diagram of leaf measurements, (*b*) common beech, mean value of $\alpha = 40.8°$, (*c*) hornbeam, mean value of $\alpha = 42.2°$.

elastic strain energy; (4) the laminar elements between the creases are plane rigid bodies, so their deformation during unfolding can be neglected (the outstretched surface is therefore assumed to be identical to the folded one—in a real leaf the surface changes during unfolding); (5) the lamina does not grow while it is unfolding; in particular the midrib is of constant length; (6) the number of folds in the lamina is held constant at nine, an arbitrarily chosen number; and (7) the size and shape of the individual laminar elements are held constant.

The corrugation folding of the model (figure 4) is very similar to that of a real hornbeam leaf (figure 5), but there is a difference in the detail close to the midrib. In the model, the midrib zigzags out of the plane of the lamina; in the real leaf the midrib is flat within the plane. This is made possible by the detail of folding close to the midrib (figure 5*b*) where the crest and valley folds neutralize each other before they reach the main vein. In addition, the second assumption implies two further factors: (i) as α decreases, the width of the lamina between the secondary veins decreases proportionally, and similarly, when α increases, so does the width; (ii) as α decreases, the length of the secondary veins increases if the width of the lamina stays constant.

For the numerical simulation, O-x,y,z coordinates were adopted (figure 4). The xz plane is symmetrical and the origin, O, is defined as the boundary point between the petiole and the midrib. The opening angle, θ, is defined as the angle between the plane of symmetry and the first element of the lamina (figure 4). Before the leaf starts unfolding, $\theta = 0°$; when the leaf is fully unfolded $\theta = 90°$. The x' axis indicates a direction of expansion of the leaf or midrib which changes during folding.

(b) ***Vector analysis***

The model (figure 4) is developed from the repetition of a simple structure with four creases where the crest or valley folds reach the midline of the model (figure 6). Once a number of properties of this configuration have been obtained, they can be generalized to the calculation of whole leaf unfolding. It may be helpful at this point to construct a paper model to observe the mechanism. Instructions are given in Appendix 1.

Let us consider the relationship between the opening angle and other parameters in this simple structure. Figure 6*a,b* gives the entire four-folded structure, and shows how the four folds (three valley folds and a crest fold) form the basic unit. Note especially the angles α and θ. Two planes are marked (I, II). Plane I will always be parallel to the x direction; if the middle sketch in figure 4 is compared with a staircase, the treads are all in plane I, the risers are all in plane II. Figure 6*c* shows half of this structure; it is symmetrical across the plane xz. Lines OA and AP are valley creases and AQ is a crest crease.

Two unit vectors, **AP** and **AQ**, on the creases, are given by the following:

$$\mathbf{AP} = p_x\boldsymbol{i} + p_y\boldsymbol{j} + p_z\boldsymbol{k} = \cos\alpha\boldsymbol{i} + \sin\alpha\sin\theta\boldsymbol{j} + \sin\alpha\cos\theta\boldsymbol{k} \quad (1)$$

$$\mathbf{AQ} = q_x\boldsymbol{i} + q_z\boldsymbol{k}, \quad (2)$$

where $\boldsymbol{i}$, $\boldsymbol{j}$ and $\boldsymbol{k}$ are the unit vectors in the x, y and z directions, respectively. The components of the vector **AQ** in x and z directions, q_x and q_z, are unknown. Since the angle between **AP** and **AQ** is α and their lengths are unity, the scalar product of **AP** and **AQ** is given by:

$$\mathbf{AP}\cdot\mathbf{AQ} = q_x\cos\alpha + q_z\sin\alpha\cos\theta = |\mathbf{AP}||\mathbf{AQ}|\cos\alpha = \cos\alpha. \quad (3)$$

Because **AQ** is a unit vector,

$$q_x^2 + q_z^2 = 1. \quad (4)$$

Solving equations (3) and (4) for q_x and q_z gives

$$q_x = [(1-h^2)/(1+h^2)],\ q_z = 2h/(1+h^2), \quad (5)$$

where $h = \tan\alpha\cos\theta$. By using these equations, the midrib element angle, ξ, defined as the angle between the x axis and the midrib (figure 6), can be expressed as

$$\xi = \tan^{-1}(q_z/q_x). \quad (6)$$

Equations (5) or (6) give the direction of the crest crease AQ when θ is known.

To expand these calculations to take account of the entire leaf, it is necessary to estimate the angle between plane II and the xz plane, θ' (figure 6*b*). Consider two lines perpendicular to AQ, i.e. BP and BC. The vector $\mathbf{BP} = \mathbf{AP} - \mathbf{AB}$ and $\mathbf{AB} = (|\mathbf{AP}|\cos\alpha)\mathbf{AQ}$. Therefore,

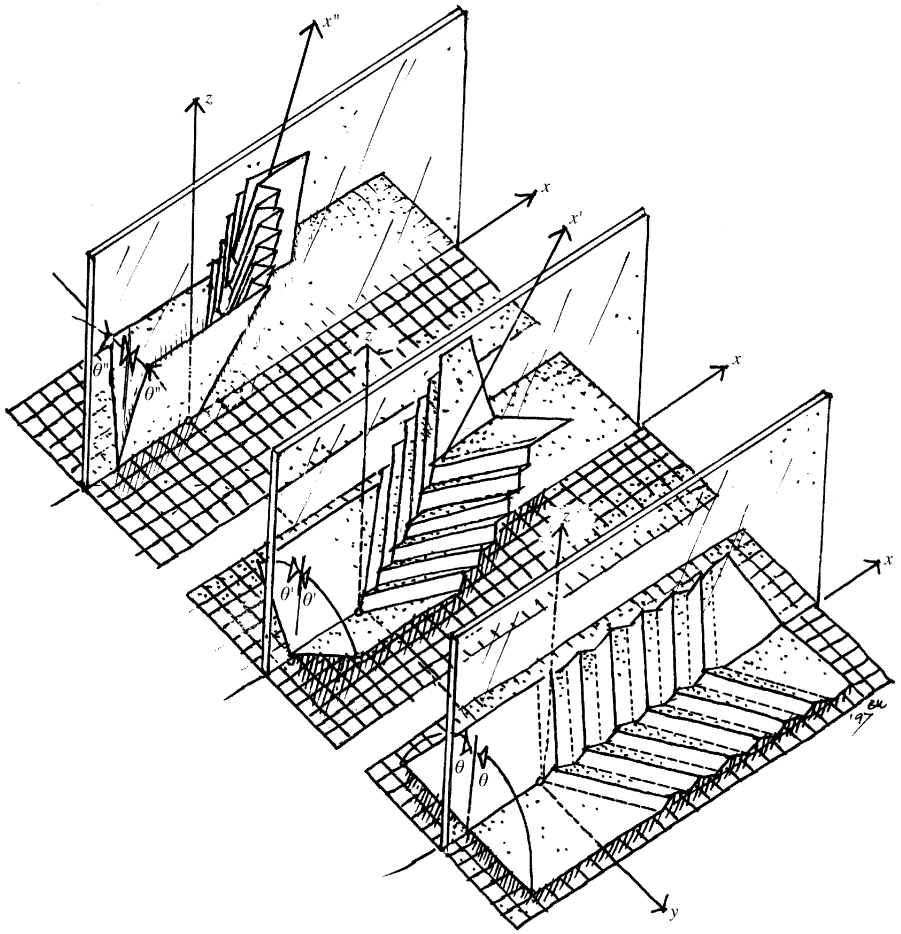

Figure 4. Corrugated model (simple form of 'Miura-Ori') and coordinates used for simulation. Three positions with different values of θ show how the model opens.

$$\mathbf{BP} = b_x\boldsymbol{i} + b_y\boldsymbol{j} + b_z\boldsymbol{k}$$
$$= \{(1 - q_x)\cos\alpha\}\boldsymbol{i} + \sin\theta\boldsymbol{j} + (\sin\alpha\cos\theta - q_z\cos\alpha)\boldsymbol{k}. \quad (7)$$

The vector **BC** is on the xz plane and perpendicular to **AQ**. If **BC** is assumed to be a unit vector, then

$$\mathbf{BC} = -q_z\boldsymbol{i} + q_x\boldsymbol{k} \quad (8)$$

because of equation (4). Taking the scalar product of **BP** and **BC** and using equations (5) and (7), $\cos\theta$ can be obtained as follows:

$$\cos\theta = (-q_z b_x + q_x b_z)/(\sqrt{b_x^2 + b_y^2 + b_z^2})$$
$$= -\cos\theta = \cos(\pi - \theta). \quad (9)$$

Therefore θ' does not depend on the vein angle α. If the opening angle of plane II (i.e. the angle through which it has rotated from the xz plane during deployment—refer to figure 4 and your model), θ_2, is defined such that $\theta_2 = \pi - \theta - \theta'$, θ_2 becomes equal to θ. Then if the opening angles of elements with even order number are defined as well as θ_2, the opening angles of all corrugated elements are the same.

Since the opening angle of the second element II is determined from equation (9), the direction of third partial midrib can be obtained using equation (5) and the technique of coordinate transformation. By repetition of this procedure, the locations of all creases and intersection points in three-dimensional space can be determined.

(c) *Numerical models*

To check the effect of differences in leaf shape on the manner of unfolding, two types of numerical model were analysed (figure 7): (i) a double parallelogram (model 1); and (ii) a double trapezium (model 2). The midrib length and half-width of both models are 108 and 20 mm, respectively. The leaf area fully unfolded, A_0, is 4320 mm^2 in model I and 2934 mm^2 in model 2. A solid line indicates a crest crease and a broken line shows a valley crease. Since the number of creases in a half side, n, is equal to eight, the total number of nodes on the midrib is ten, and the distance between nodes is 12 mm (figure 7). Each model was computed several times with different vein angles. The outline shape of model 2 is fixed; therefore the length of the model, L, is also fixed. However, the shape of model 1 depends on the vein angle, and L increases with decreasing α.

4. SIMULATION RESULTS AND DISCUSSION

(a) *Leaf shape fully folded*

The side views of model 2 leaves fully folded are shown in figure 8*a*. The portions shaded indicate the reverse surface. The shape and the area of side views thus depend on the vein angle, α. Leaves with larger α can be folded more compactly. The area ratios, A_F* (A_F* = A_F/A_0,

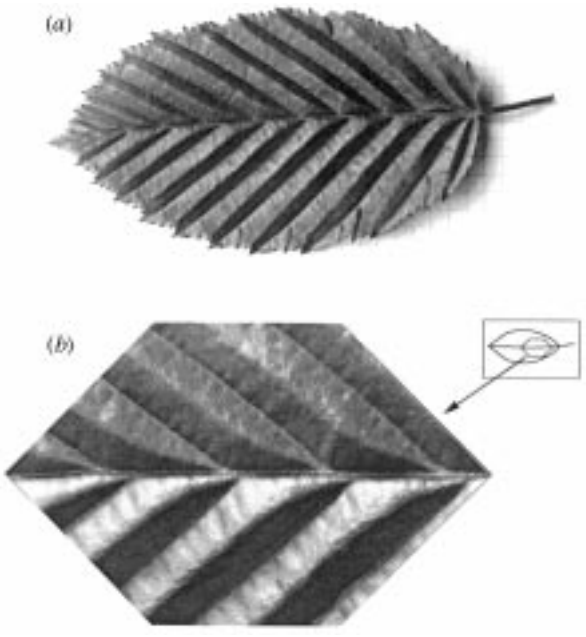

Figure 5. Hornbeam leaf showing (*a*) relatively regular corrugation, and (*b*) three-dimensional structure close to the midrib.

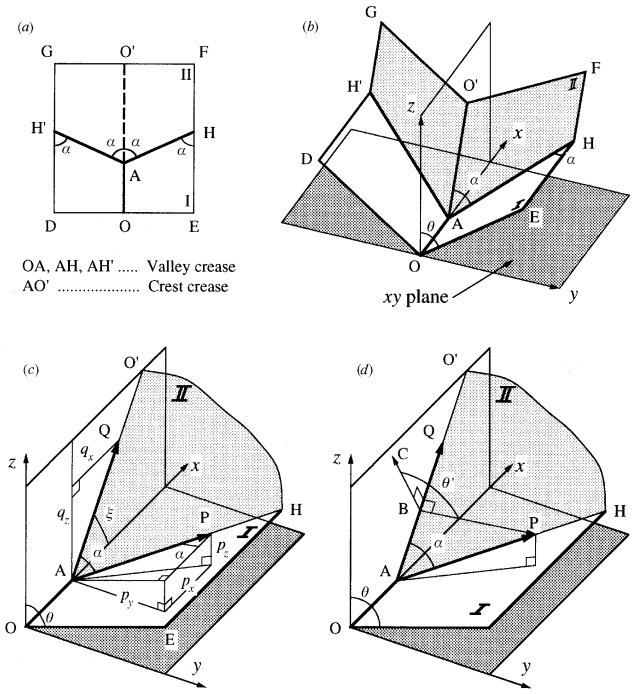

Figure 6. Schematic drawing for vector analyses: (*a*) the undeveloped structural unit, (*b*) the structural unit folded (cf. figure 4), (*c*) relation between α and lamina partial planes I and II, and (*d*) relation between θ, θ' and lamina partial planes I and II.

where A_F is the lateral area of model leaves and A_0 is the unfolded area), are shown in figure 8*b*. In both models, the leaf with $\alpha=45^\circ$ has the largest A_F. The A_F of the leaf with $\alpha=85^\circ$ is about half of that with $\alpha=45^\circ$. By folding with $n=8$, the surface area of the leaf can be reduced to 10–20% of an unfolded leaf. This reduction depends on the number of creases.

The aspect ratio of the side views of folded leaves, r^*, can be defined as $r^* = L_F/H_F$, where L_F and H_F are the length and width in side view (figure 8*a*). Figure 8*c* shows this aspect ratio for various vein angles. For both models, r^* decreases with the increase of vein angle. A small r^* appears to be more suitable for storing folded leaves into a small space. Therefore, leaves with large α (75–85°), have an advantage for compact housing in the bud.

(b) *Leaf shape during unfolding*

To examine the behaviour of unfolding leaves, the shapes of leaf models projected on to the $x'y$ plane (figure 4) were calculated at several opening angles, θ. Figure 9 shows the half-leaf of model 2 leaves with two different vein angles, $\alpha=30^\circ$ and 85°, for comparison. In the leaf with $\alpha=30^\circ$ (figure 9*a*), the change of length (in the x' direction) is not so large; in general, the width of the leaf increases as the opening angle increases. The leaf with $\alpha=85^\circ$ (figure 9*b*) extends transversely (y direction) predominantly in the early stage of unfolding and then elongates dramatically in the last stages of opening (θ is 70–90°). Although the shape of the leaf when it is fully unfolded is the same, the area of the model leaf with $\alpha=85^\circ$ during unfolding appears to be much smaller than that with a 30° vein angle over the range θ is 10–80°. Figure 10 shows the change of projected leaf area ratio, A^* ($=A/A_0$), for model 2 leaves during unfolding. The leaf model with $\alpha=30^\circ$ already has 60% of the fully unfolded area, A_0, at $\theta=40^\circ$. However, at the same value

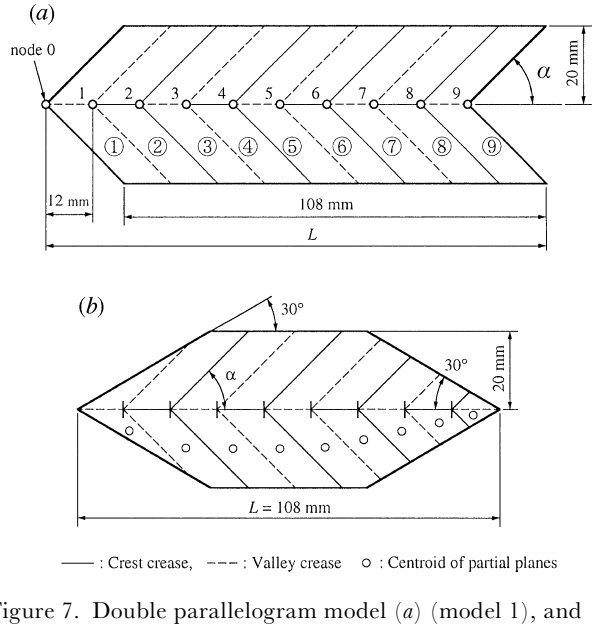

Figure 7. Double parallelogram model (*a*) (model 1), and double trapezium model (*b*) (model 2) used for numerical simulations. (*a*) $A_0=4320\,\text{mm}^2$, vein angle $\alpha=15^\circ$, 30°, 45°, 60°, 75°, 85°. (*b*) $A_0=2934\,\text{mm}^2$, vein angle $\alpha=30^\circ$, 45°, 60°, 75°, 85°.

of θ, the model with $\alpha=85^\circ$ has less than 10% of A_0. A similar tendency was noted from the results of model 1.

This highlights several factors relevant to the biology of the process of unfolding and deployment of a leaf. Timing is presumably important only where the habitat has annual cycles. Away from tropical areas where there is a

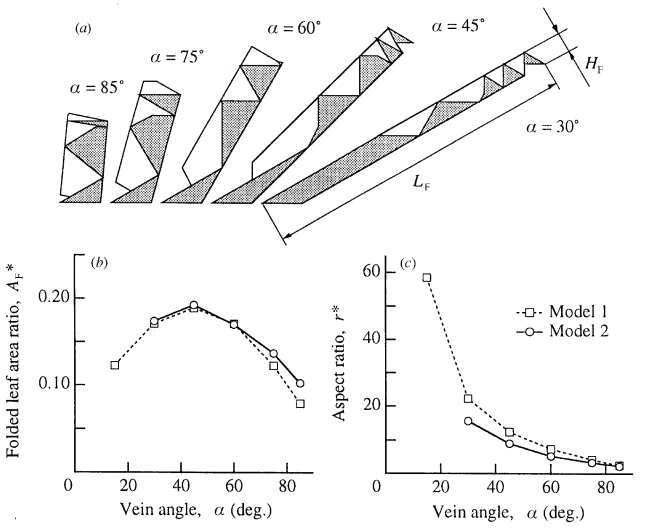

Figure 8. Leaf model shapes fully folded. (*a*) Side views of folded model leaves with several vein angles (model 2). (*b*) Relation between folded leaf ratios, $A_F^* = A_F/A_0$, and vein angles, α. (*c*) Relation between aspect ratio, $r^* = L_F/H_F$, of side views of folded leaves and vein angles, α.

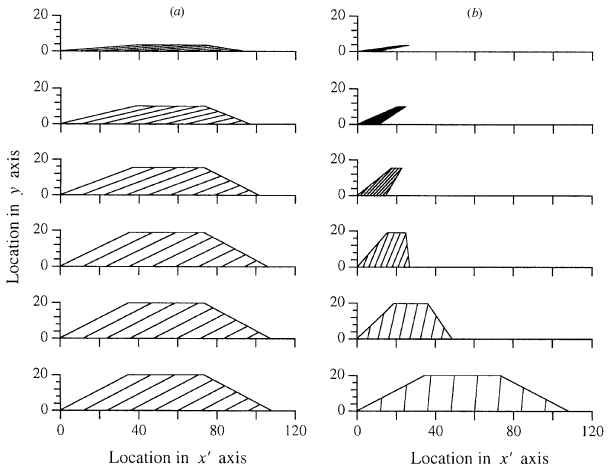

Figure 9. Half-model leaves with α of (*a*) 30° and (*b*) 85° during unfolding (model 2). For parts (*a*) and (*b*) and from top to bottom, $\theta = 10°$, 30°, 50°, 70°, 80° and 90°, respectively.

limited growing season, one might expect the leaf to be deployed as quickly as possible once the temperature and light intensity become favourable. However, this will expose the leaf to damage by late frosts, and attract herbivores early in the season when green food is scarce. A leaf that exposes its full area only late in the process of expansion might be at an advantage in defending itself from this sort of damage, but is then not able to photosynthesize effectively during the early stages of expansion, and must rely on nutrients stored from the previous season. However, the strategy of opening fully only in the last stages of deployment may be an advantage in arid areas since the leaf can retain a very small surface area when partially opened, remain inactive at this stage, and then achieve full deployment of the lamina much more quickly when the rains come.

(c) *Energy required during unfolding*

Another parameter for comparing deployment of the models examined here is the kinetic energy dissipated during unfolding. The mathematics are not presented here because the leaves open so slowly that the kinetic energy cannot be an important biological parameter. It is, however, likely to be important in a quickly deployable artificial structure based on a leaf pattern, and does show some interesting differences that we aim to cover at a later date. More energy is required as the opening angle, θ, increases (figure 11) towards the final stages of unfolding.

(d) *Final comments*

We have not explored a number of other linked variables, such as the length of the secondary vein and the width of the lamina between the secondary veins and, of course, the factors outlined in the list of assumptions. The present model takes no account of elastic buckling mechanisms in the laminar segments between the veins or elastic bending in the veins themselves. The simplified model at which we arrive is very much the result of a mathematical analysis that remains to be integrated into a biological context, in particular taking into account the effects of growth. Since a number of the parameters are linked (for instance α and the length of secondary veins for a given width of lamina), there is scope for optimization studies on the design of the real leaf. These optimizations may be expressed before or after the emergence of the leaf from the bud.

5. CONCLUSIONS

We conclude that (1) common beech and hornbeam have corrugated leaves whose vein angles range from 30–50° from the tip to the petiole; (2) a leaf with large vein angles (75–85°) can be folded more compactly than one with small angles (30–45°); (3) a leaf with small vein angles can attain a relatively large deployed area in the early stages of unfolding; and (4) the kinetic energy required for the full unfolding increases with vein angle.

We thank Mrs B. Stühlen for help with observations of leaves unfolding in the spring and Dr Thomas Speck for useful comments during refereeing.

APPENDIX 1. HOW TO MAKE A LEAF MODEL

Take a sheet of paper about twice as long as wide (e.g. 10 cm × 20 cm) and fold it in half lengthways. Taking the fold as the datum, mark a line at about 60° to the datum about 2 cm from one end and fold the sheet along this line. Mark another line at the same angle about 1 cm further along the sheet and fold the paper back again. This gives the shape shown on the extreme left in figure 12. Iteration of this process leads to the second shape which, stretched out, leads to the third shape. The sheet is then unfolded about the long axis, and the paper refolded along these creases to give the shape shown to the right of figure 12. This involves converting valley folds to crest folds or vice

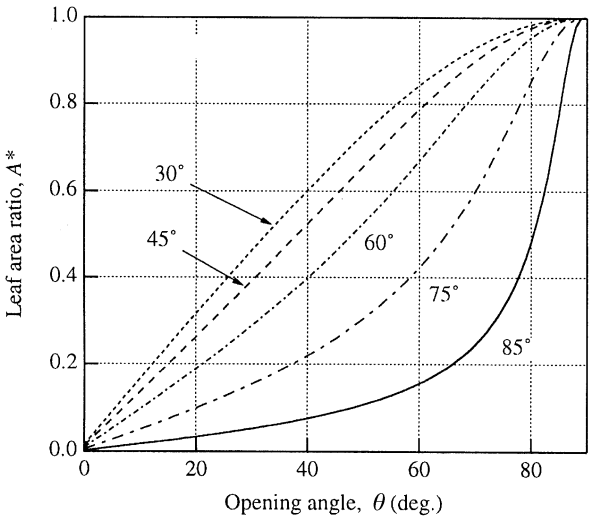

Figure 10. Relationship between leaf area ratio, A^*, and opening angle, θ (model 2).

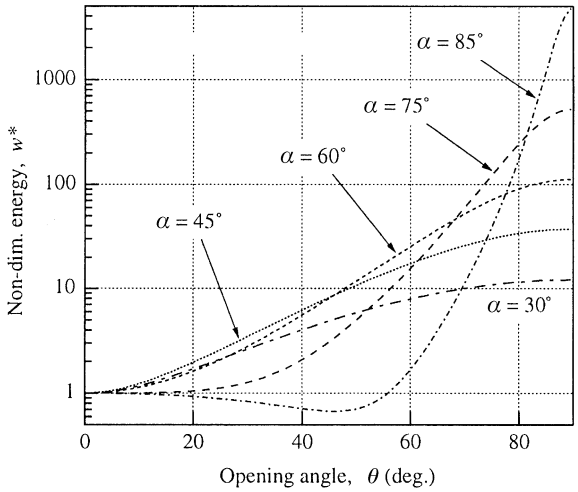

Figure 11. Changes in kinetic energy of model 2 leaves in unfolding.

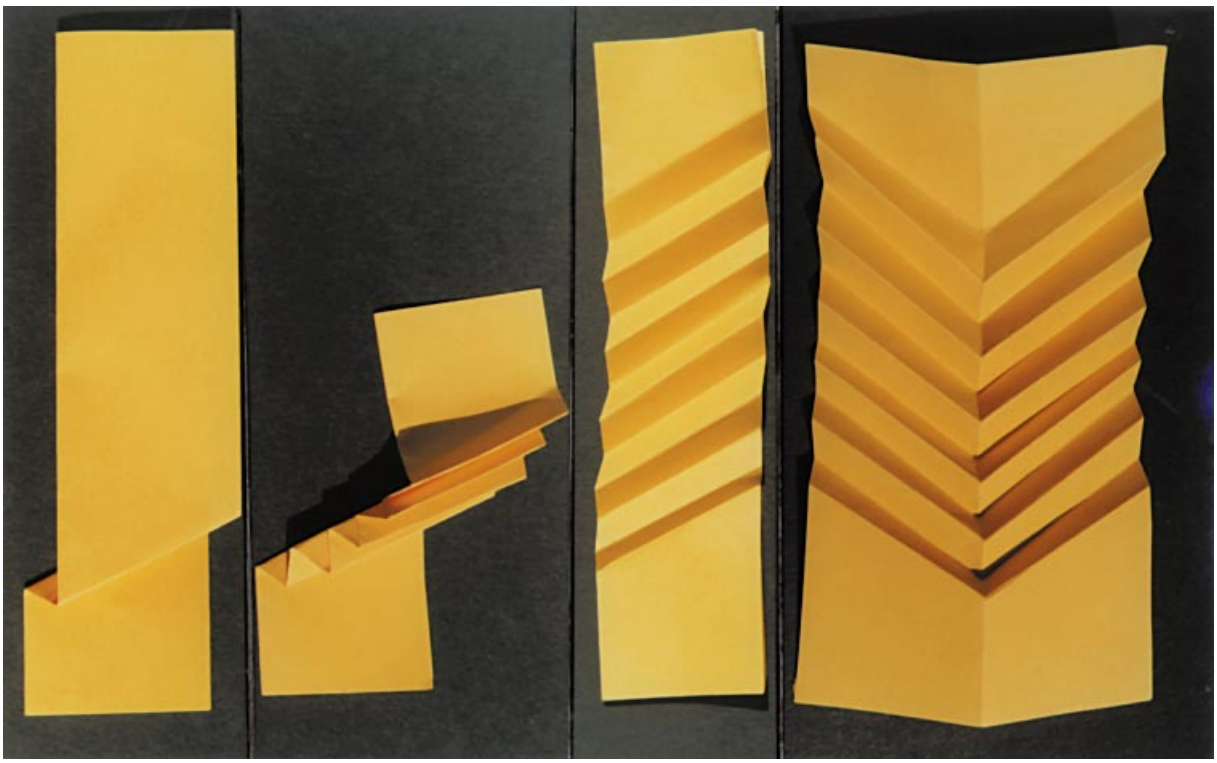

Figure 12. Stages in making 'ha-ori' (leaf-folding).

versa along the sheet. Take each segment of the leaf separately, emphasizing the correct folds before going on to the next. The action of the model is shown in figure 4.

REFERENCES

Brackenbury, J. H. 1994 Wing folding and free-flight kinematics in Coleoptera (Insects): a comparative study. *J. Zool. Lond.* **232**, 253–283.

Calladine, C. R. 1978 Buckminster Fuller's 'Tensegrity' structures and Clerk Maxwell's rules for the construction of stiff frames. *Int. J. Solids Struct.* **14**, 161–172.

Delarue, J. M. 1991 Minimal folding configurations. *Proc. 2nd Int. Symp. SFB 230 Part 2, Stuttgart*, pp. 31–41.

Guest, S. D. & Pellegrino, S. 1992 Inextensional wrapping of flat membranes. In *Proc. 1st Int. Sem. Struct. Morphol.* (ed. R. Motro & T. Wester), pp. 203–215. Montpellier.

Guest, S. D. & Pellegrino, S. 1994*a* The folding of triangulated cylinders. I. Geometric considerations. *J. Appl. Mech. ASME* E **61**, 773–777.

Guest, S. D. & Pellegrino, S. 1994*b* The folding of triangulated cylinders. II. The folding process. *J. Appl. Mech. ASME* E **61**, 778–783.

Guest, S. D. & Pellegrino S. 1996 The folding of triangulated cylinders. III. Experiments. *J. Appl. Mech. ASME* E **63**, 77–83.

Haas, F. 1994 Geometry and mechanics of hind-wing folding in Dermaptera and Coleoptera. M.Phil. thesis, University of Exeter, UK.

Herbig, A. & Kull, U. 1991 Leaves and ramification. In *Proc. 2nd Int. Symp. SFB 230 Part 2, Stuttgart*, pp. 109–117.

Kresling, B. 1991 Folded structures in nature—lesson in design. *Proc. 2nd Int. Symp. SFB 230 Part 2, Stuttgart*, pp. 155–161.

Kresling, B. 1995 Plant 'design': mechanical simulations of growth patterns and bionics. *Biomimetics* **3**, 105–120.

Miura, K. 1980 Method of packaging and deployment of large membranes in space. *Proc. 31st Congr. Int. Astronaut. Federation, IAF-80-A 31 Tokyo*, pp. 1–10.

Miura, K. & Natori, M. 1985 2-D array experiment on board a space flyer unit. *Space Solar Power Rev.* **5**, 345–356.

Miura, K. 1993 Concepts of deployable space structures. *Int. J. Space Struct.* **8**, 3–16.

Kesel, A. B. 1994 The insect wing—a multifunctional mechanical system. *Proc. 3rd Int. Symp. SFB 230, Stuttgart*, pp. 181–184.

Unda, J., Weisz, J., Rivacoba, J. & Urfen, I. R. 1994 Family of deployable/retractable structures for space application. *Acta Astro.* **32**, 767–784.

Wootton, R. J. 1981 Support and deformability in insect wings. *J. Zool. Lond.* **193**, 447–468.